Mapping Plant Functional Types at Multiple Spatial Resolutions Using Imaging Spectrometer Data

Abigail N. Schaaf
*Department of Geography, University of Utah,
260 South Central Campus Drive, Room 270,
Salt Lake City, Utah 84112 and U.S. Forest Service,
Remote Sensing Applications Center,
2222 W. 2300 South, Salt Lake City, Utah 84119*

Philip E. Dennison[1] and Gregory K. Fryer
Department of Geography, University of Utah, 260 South Central Campus Drive, Room 270, Salt Lake City, Utah 84112

Keely L. Roth and Dar A. Roberts
Department of Geography, University of California Santa Barbara, Santa Barbara, California 93106

Abstract: Imaging spectrometer data have been used to map plant functional types (PFTs—plant species grouped by similarities in their resource use, ecosystem function, and responses to environmental conditions) at spatial resolutions of 30 m and finer, but not at coarser spatial resolutions that may be necessary for global PFT mapping. This study uses spatially resampled Airborne Visible InfraRed Imaging Spectrometer (AVIRIS) data acquired over the Wasatch Mountains of northern Utah, USA to examine changes in PFT classification accuracy as spatial resolution is degraded from 20 to 60 m. Accuracy was dependent on the spatial resolution of the classified data and the spatial resolution of endmembers used in the multiple endmember spectral mixture analysis classifier.

INTRODUCTION

Mapping, monitoring, and identifying changes in vegetation cover are critical for improving understanding of global change phenomena. Vegetation mapping using remotely sensed data has been applied to measure ecosystem response to climate change, disturbance, and invasive species (Nemani et al., 1996; Myneni et al., 2001; Chambers et al., 2007; Dennison et al., 2009). Vegetation mapping is also an important component in the support of management of natural resources, such as inventory assessment, fuels management, and wildlife habitat characterization (Bobbe et al., 2001). To facilitate modeling of vegetation responses to ecosystem change, many

[1]Corresponding author: email: dennison@geog.utah.edu

GIScience & Remote Sensing, 2011, **48**, No. 3, p. 324–344. DOI: 10.2747/1548-1603.48.3.324

ecologists group plant species into "plant functional types" (PFTs; Diaz and Cabido, 1997). PFTs are groupings of plant species based not on phylogenetic relationships, but rather on similarities in their resource use, ecosystem function and responses to environmental conditions (Walker, 1992). This simplified and generalized structure of vegetation classification has been found to be valuable for understanding natural and human-induced environmental changes and the processes behind them (Bugmann, 1996; Woodward and Cramer, 1996; Diaz Barradas et al., 1999; Lavorel and Garnier, 2002).

Imaging spectroscopy, which measures reflected solar radiance using a large set of narrow, contiguous spectral bands, has shown particular promise for mapping plant taxa and functional types (Martin et al., 1998; Roberts et al., 1998; Dennison and Roberts, 2003a; Clark et al., 2005; Plourde et al., 2007; Asner et al., 2008). The United States National Research Council has recommended a spaceborne global survey mission to measure ecosystem response to environmental change, including an imaging spectrometer capable of mapping PFTs (National Research Council, 2007). While previous studies have used 30 m or finer spatial resolution imaging spectrometer data for mapping vegetation, a global mapping mission is likely to require a coarser spatial resolution due to tradeoffs between repeat interval, swath width, and spatial resolution. The VSWIR spectrometer, one component of the proposed HyspIRI mission, would have a 60 m spatial resolution.

Multiple endmember spectral mixture analysis (MESMA) has been successfully used as a vegetation and PFT classification method for imaging spectrometer data at sub–30 m spatial scales (Roberts et al., 1998; Dennison and Roberts, 2003a, 2003b; Li et al., 2005; Youngentob et al., 2011). This research uses MESMA to classify PFTs at three spatial resolutions for the Wasatch Mountains of northern Utah, USA. PFT classifications at 20, 40, and 60 m spatial resolution demonstrate the impact of changing spatial resolution on map accuracy, and provide important context for understanding how future spaceborne imaging spectrometers can contribute to vegetation mapping and global process modeling.

BACKGROUND

Vegetation Mapping Using Imaging Spectrometer Data

Imaging spectrometer data have been used to map vegetation in a variety of ecosystems. Martin et al. (1998) classified forest cover types at the stand level from Airborne Visible InfraRed Imaging Spectrometer (AVIRIS) reflectance data acquired in Harvard Forest in central Massachusetts. Their work demonstrated that imaging spectroscopy could successfully discriminate 11 forest classes with 75% accuracy. Thenkabail et al. (2004) utilized data from the spaceborne imaging spectrometer Hyperion to classify nine land cover types ranging from slash-and-burn farms to undisturbed tropical rain forest across an expanse of six different ecoregions in West Africa. Using stepwise linear discriminant analysis, they achieved an overall accuracy of 96% using 23 Hyperion bands. Clark et al. (2005) examined the species-level separability of seven tropical rainforest species using canopy-level imaging spectrometer data. Maximum likelihood classification yielded an 88% overall accuracy. Youngentob et al. (2011)

mapped eucalyptus forest by applying MESMA to continuum-removed HyMap image spectra, and achieved 81% accuracy at the subgeneric level.

Previous work in shrublands has focused on mapping shrub taxa in southern California chaparral. Roberts et al. (1998) used MESMA to map a variety of chaparral species in the Santa Monica Mountains of California. Dennison and Roberts (2003a) mapped five chaparral PFTs in the Santa Ynez Mountains using MESMA, resulting in a 93% overall accuracy. Dennison and Roberts (2003b) examined the effects of vegetation phenology endmember selection for MESMA. Seasonality was found to impact the spectral shape of the selected endmembers and the confusion between endmembers increased as soil water balance changed from positive to negative.

Imaging spectrometer data have also been extensively utilized for mapping invasive species such as tamarisk (*Tamarix* spp.) (Narumalani et al., 2006; Hamada et al., 2007), horse tamarind (*Leucaena leucocephala*) (Tsai et al., 2005), iceplant (*Carpobrotus edulis*), jubata grass (*Cortaderia jubata*), fennel (*Foeniculum vulgare*) and giant reed (*Arundo donax*) (Ustin et al., 2002; Underwood et al., 2003), leafy spurge (*Euphorbia esula*) (Everitt et al., 1995; Williams and Hunt, 2002), and hoary cress (*Cardaria draba*) (Mundt et al., 2005). The ability of imaging spectrometer data to detect invasive species among a mixed landscape of native vegetation has been successful mainly due to the fact that the invasive species can often have a distinct spectral signature when compared against native vegetation.

Multiple Endmember Spectral Mixture Analysis

Spectral mixture analysis (SMA) models the fractional cover of "endmembers" (representing pure land cover types within an image pixel) along with a shade endmember that is used to adjust for shadowing and topographic shading (Adams et al., 1993). Linear SMA assumes that the spectra of the land cover types in an instantaneous field of view (IFOV) combine linearly, and that the spectral contribution of each land cover type is proportional to its relative abundance within the pixel IFOV. Linear SMA is based on the following equation:

$$\rho'_{\lambda} = \sum_{i=1}^{N} f_i {}^* \rho_{i\lambda} + \varepsilon_{\lambda}, \tag{1}$$

where ρ'_{λ} is the reflectance of a given pixel and is calculated as the sum of the reflectance of each endmember ($\rho_{i\lambda}$) within the pixel, multiplied by its fractional cover (f_i); N is the number of endmembers; and ε_{λ} is the residual error. Model fit is assessed using root mean square error (RMSE), which is calculated as:

$$RMSE = \left(\frac{\sum_{b=1}^{M} (\varepsilon_{\lambda})^2}{M} \right)^{1/2}, \tag{2}$$

where b is the sequential band number and M is the total number of bands. RMSE represents the extent to which modeled reflectance matches measured reflectance for each pixel spectrum.

Standard SMA uses a uniform set of endmembers (measured in the laboratory or field or extracted from the image) for the entire image, and cannot account for spectral variability introduced by multiple vegetation types, multiple soil types, or within-class spectral variability. Roberts et al. (1998) developed MESMA to allow endmembers to vary on a per-pixel basis. MESMA requires a more extensive spectral library than SMA, allowing multiple potential endmembers that capture the spectral variability of a single land cover type. Unlike SMA, two-endmember MESMA (one shade endmember and one non-shade endmember) can be used as an image classification algorithm. MESMA using three or more endmembers can be used to measure fractional cover. MESMA has been used to map southern California shrublands (Roberts et al., 1998; Dennison and Roberts, 2003a, 2003b), eucalypt forest (Youngentob et al., 2011), coastal salt marsh (Li et al., 2005), soils and landforms (Okin et al., 2001; Ballantine et al., 2005), snow grain size (Painter et al., 2003), urban land cover (Rashed et al., 2003; Powell et al., 2007), fire temperature (Dennison et al., 2006; Dennison and Matheson, 2011), and planetary surface composition (Li and Mustard, 2003; Johnson et al., 2006). As a classification method, two-endmember MESMA is well-suited for mapping PFTs in mountainous terrain. The inclusion of a shade endmember adjusts for variations in direct irradiance caused by topography.

Several approaches to endmember selection have been developed for MESMA in order to produce a parsimonious set of endmembers representing different vegetation types. Roberts et al. (2003) proposed a count-based approach to endmember selection, where the endmembers that modeled the largest number of spectra within a spectral library class were selected. Dennison and Roberts (2003a) developed a method for selecting a set of endmembers that is more spectrally representative of each land cover class for use in MESMA. This is done by using a metric called Endmember Average RMSE (EAR), which allows each spectrum within a class to model all other spectra within the class using linear SMA. The spectrum with the minimum mean RMSE is then selected as an endmember. Dennison et al. (2004) introduced Minimum Average Spectral Angle (MASA), which functions similarly to EAR, but uses spectral angle (Kruse et al., 1993) as the selection metric. In practice, all of these past approaches to endmember selection for MESMA require some degree of subjectivity in selecting the single "best" set of endmembers for classification.

METHODS

Study Area

Four PFTs were mapped using AVIRIS data covering a portion of the Wasatch Mountain Range in northern Utah, USA (Fig. 1). The range emerges directly east of Salt Lake City, Utah (40°46′ N, 111°58′ W) spanning roughly 260 km from north to south. The AVIRIS scene used for this study covers the western side of the Wasatch Range adjacent to the Salt Lake Valley. Classification focused on the subset of the scene between U.S. Interstate 80 and Little Cottonwood Canyon, indicated by the dashed box in Figure 1. The Wasatch Range within the study area rises from approximately 1500 m elevation at the edge of the Salt Lake Valley up to summits higher

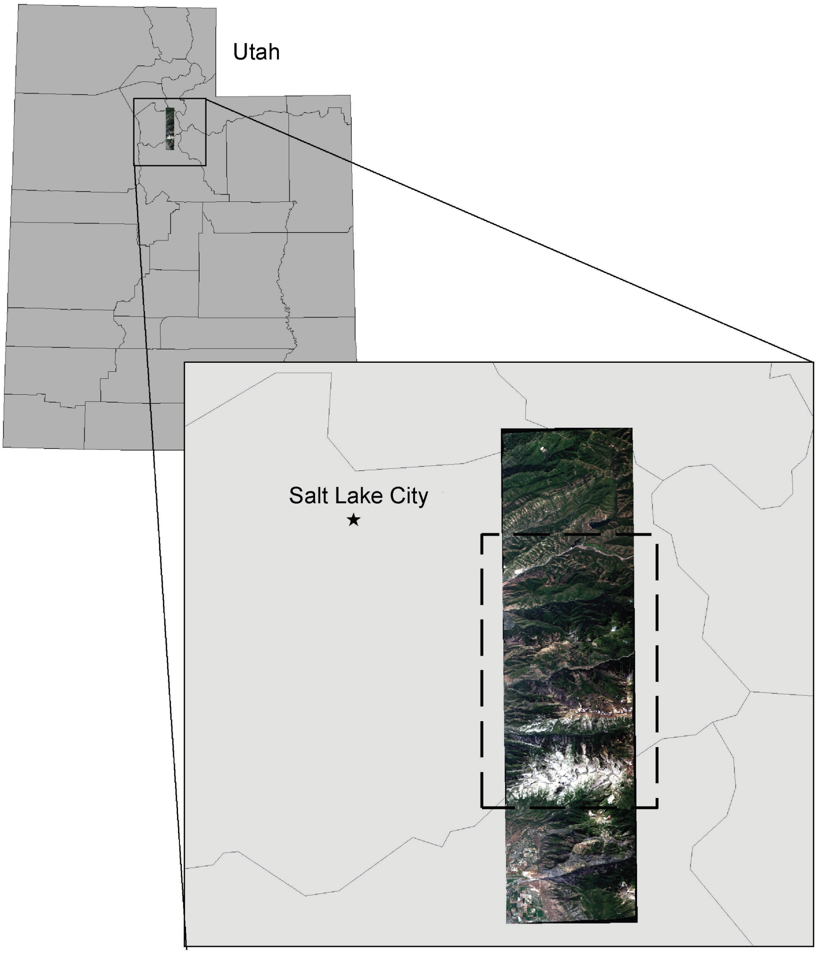

Fig. 1. Map showing the AVIRIS flight line and the location of the study area (dashed box).

than 3400 m (Fig. 2). The 28 km × 11 km study area is crossed by multiple east-west–oriented canyons. Shrub cover dominated by Gamble oak (*Quercus gambelii*) is common at lower elevations. Higher elevations are dominated by tree species including aspen (*Populus tremuloides*), Douglas fir (*Pseudotsuga menziesii*), white fir (*Abies concolor*), subalpine fir (*Abies lasiocarpa*), limber pine (*Pinus flexilis*), and Engelmann spruce (*Picea engelmannii*), along with grass and herbaceous vegetation cover in mountain meadows.

AVIRIS and NAIP Data

The AVIRIS image used for this study was acquired on August 5, 1998. AVIRIS has 224 bands with an approximate bandwidth of 10 nm, and covers a spectral range of 350–2500 nm. The sensor was flown on the NASA ER-2 platform at an altitude of 21 km, producing an image swath width of approximately 11 km and a ground IFOV of

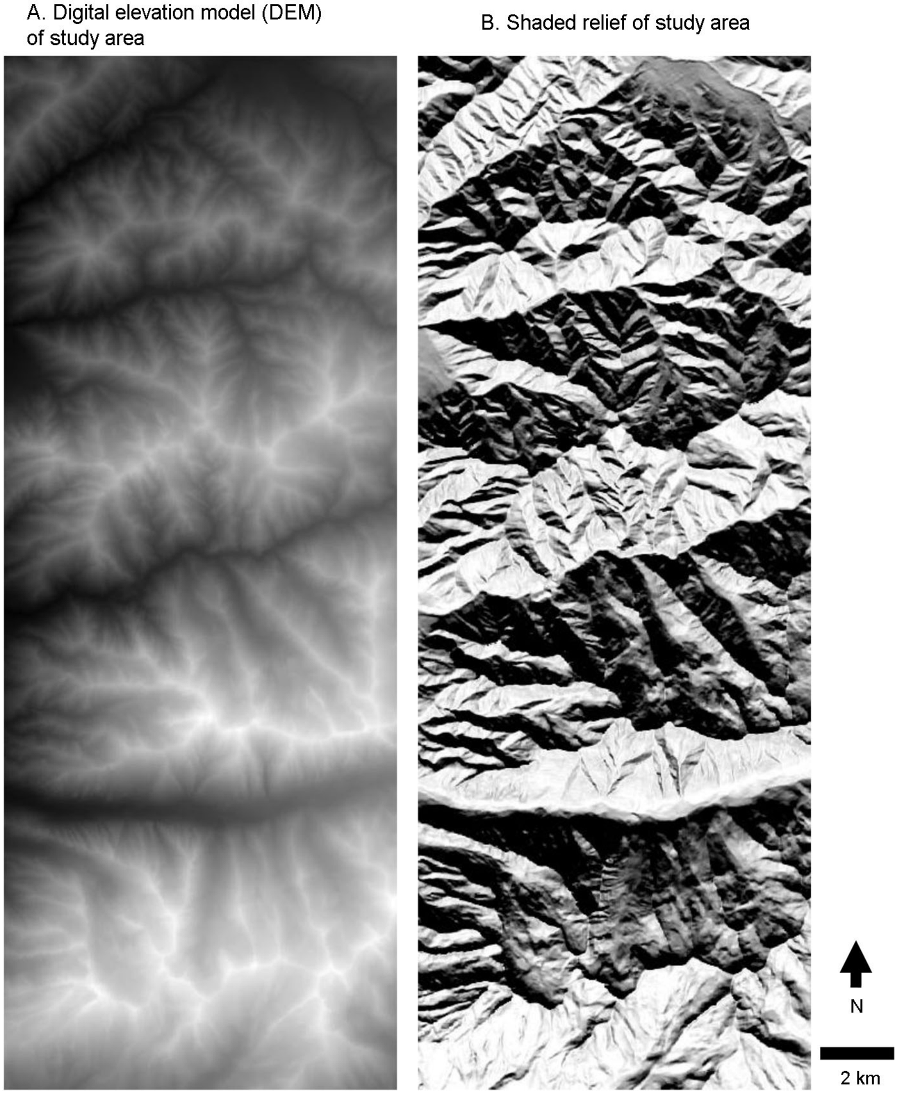

Fig. 2. A. Elevation within study area, scaled between 1480 m and 3460 m. B. Shaded relief within the study area, using an illumination zenith of 45° and a due-south illumination azimuth. South-facing slopes appear bright, and north-facing slopes appear dark.

approximately 20 m. Digital orthophotography from the National Agriculture Imagery Program (NAIP) was used to register the AVIRIS image and aid in selection of ground reference polygons that were used to train and assess the accuracy of the MESMA classification. NAIP 1 m spatial resolution color and color infrared aerial photography was acquired over the study area on August 10 and August 31, 2006. The eight-year period between acquisition of the AVIRIS and NAIP data was not optimal, but no major disturbance (e.g., fires, logging) or shifts in the spatial distributions of PFTs were noted to have occurred during this time period within the study area.

The 20 m AVIRIS calibrated radiance image was registered to an NAIP true-color orthophoto resampled to a 20 m spatial resolution. A total of 885 tie points were established to register the AVIRIS image to the resampled NAIP image. Delaunay triangulation with nearest neighbor resampling was used to warp the AVIRIS image. The registered AVIRIS radiance image was then degraded from its original spatial resolution of 20 m to 40 m and 60 m using spatial averaging. For example, the mean of four 20 m pixel spectra was calculated to create the 40 m image, and the mean of nine 20 m pixel spectra was calculated to create the 60 m image. Each image was then separately corrected to apparent surface reflectance using the FLAASH (Anderson et al., 2002) atmospheric correction package in ENVI (ITT Visual Information Solutions). The mid-latitude summer atmospheric and rural aerosol models were used, and visibility was set to 30 km based on path radiance within the radiance image. Water vapor retrieval was applied using the 1135 nm water vapor absorption feature. The 20, 40, and 60 m apparent surface reflectance images produced by FLAASH were subset from 224 bands to 190 bands, dropping bands that were found to have strong atmospheric water vapor absorption.

PFT Reference Data

An image segmentation algorithm (eCognition, version 7.0, Definiens Developer) was applied to the 1 m NAIP color and color infrared orthophotos to create polygons with internally similar land cover. eCognition uses an object-based approach to derive image segments (Baatz et al., 2004). Neighboring pixels are examined for their similarity based on input parameters of scale (which controls the level of desired heterogeneity), shape, and compactness. Multiple parameter configurations were tested, and best values for each parameter were empirically determined to be 90 for scale, 0.5 for shape, and 0.5 for compactness. Using these parameters, the study area was segmented into polygons that were then assigned PFT identities in the field.

Four PFTs were mapped during field work that took place over the summer of 2009. Functional types were assigned based on leaf type and life-form. The four PFT classes were broadleaf deciduous shrub (e.g., Gambel oak), broadleaf deciduous tree (primarily aspen), needleleaf evergreen tree (e.g., Engelmann spruce), and grass/herbaceous (meadows). A fifth PFT, broadleaf evergreen shrub, is present in the study area. However, the major species in this functional type, curl-leaf mountain mahogany (*Cercocarpus ledifolius*), was not found in sufficiently large stands to map at 20 m spatial resolution. A fifth rock and soil class was also mapped using the polygons generated from the NAIP data.

Polygons were required to be at least 60 m by 60 m in size and dominated by a single land cover type (at least 75% dominance) to ensure that the PFT classification by MESMA would be applicable across all of the examined spatial resolutions. Dominant PFTs were assigned to a total of 174 image polygons based on field observation. An additional 47 polygons dominated by rock and/or soil were also identified in the field and using the 1 m NAIP orthophoto. After field mapping was complete, the field polygons were randomly partitioned into a set of reference training polygons for selecting endmembers for MESMA and an independent set of post-classification accuracy assessment polygons.

The period of time between AVIRIS data acquisition (1998), NAIP data acquisition (2006), and PFT assignment (2009) was longer than desired. Unfortunately, more recent airborne imaging spectrometer data at any spatial resolution were not available anywhere within the Wasatch Range. No major disturbance, such as fires, logging, or landslides, was known to have occurred within the study area during this time period. Most of the study area is protected within the Mount Olympus and Twin Peak Wilderness Areas, and polygons directly adjacent to obvious human impacts (e.g., roads) were avoided.

Iterative Endmember Selection and MESMA Classification

Spectra were extracted from the field-validated training polygons for each of the five land cover classes using ENVI. ENVI extracts pixel spectra where the centroid of the pixel falls within a polygon. Extracted spectra from the 20, 40, and 60 m AVIRIS reflectance images were used to create separate spectral libraries for all three spatial resolutions. For each training library, an automated iterative endmember selection algorithm was then used to find the set of endmembers that produced the highest kappa value for classifying the spectra within the training library. Unlike overall accuracy, kappa accounts for agreement by chance and is a better measure of accuracy when class representation is not uniform within a dataset (Congalton, 1991). First, the algorithm compared all possible pairs of endmembers to find the two endmembers that resulted in the highest kappa value for classifying the training library using MESMA. Then all potential additional endmembers were compared for their ability to increase kappa. The endmember that increased kappa the most was added to the selected set of endmembers. Next, each endmember from the selected set was subtracted to test whether kappa further improved with endmember removal. Addition and subtraction of endmembers then continued until kappa no longer increased and the final selected set of endmembers was determined.

The endmember libraries were then used to classify the AVIRIS images using MESMA, as implemented in the ENVI add-on ViperTools (http://vipertools.org). Five combinations of endmember libraries and image resolutions were tested. Each endmember library (20, 40, and 60 m) was applied to the respective reflectance image it was extracted from. Additionally, the 20 m endmembers were applied to the 40 and 60 m AVIRIS images to assess accuracy differences resulting from using endmembers acquired from a finer resolution data source. MESMA was used to model the reflectance images with two endmember models, where the best-fit combination of a PFT endmember and a photometric shade endmember was selected for each pixel. The minimum and maximum allowable endmember fractional constraints were set to –0.05 and 1.05, respectively (Dennison and Roberts, 2003a). RMSE was constrained to below 0.025 to assign a valid model fit. Pixels that were not modeled with an RMSE of less than 0.025 with any of the endmembers in the library were categorized as unclassified.

Accuracy Assessment

Pixel-level error matrices were created for each combination of image and endmember spatial resolutions, and producer's accuracy (representing errors of omission) and user's accuracy (representing errors of commission) were calculated from each

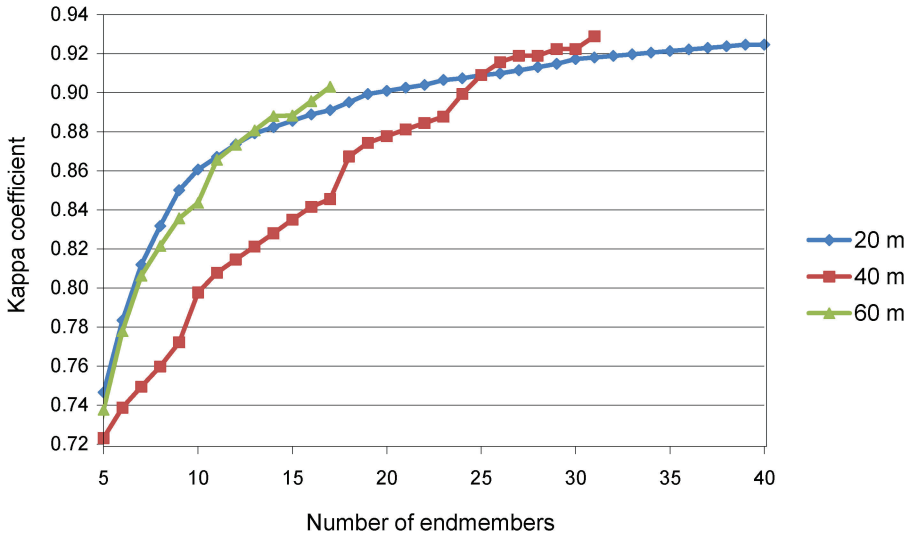

Fig. 3. Changes in kappa with the number of endmembers selected from the 20 m, 40 m, and 60 m images.

error matrix. Overall accuracy, kappa, and kappa variance were also calculated for each classification (Congalton, 1991). Kappa values close to zero indicate agreement due to chance, and as the value of kappa approaches 1 agreement is less likely to be due to chance. Kappa and kappa variance were used to calculate a Z-statistic for each pair of classifications to determine whether their kappa coefficients were significantly different at the 95% confidence level (Congalton, 1991).

RESULTS

Endmember Selection

The iterative endmember selection algorithm rapidly increased the within-library kappa until one endmember was added for each of the five classes (Fig. 3). Kappa then increased more slowly as multiple endmembers were added for each class, until a maximum kappa value was reached at each spatial resolution. This maximum within-library kappa peaked at 0.90 for the 20 m library, 0.87 for the 40 m library, and 0.89 for the 60 m library. A total of 44 endmembers were selected at 20 m, decreasing to 23 endmembers at 40 m and 19 endmembers at 60 m (Table 1).

Degrading Both Image and Endmember Spatial Resolution

In the 20 m MESMA classification, the spatial distribution of the four PFTs and the rock/soil class qualitatively coincided with topographic features (Fig. 4A). Needleleaf evergreen trees were most prevalent on north- and west-facing slopes at higher elevations. Broadleaf deciduous trees were mapped at higher elevations on the right side of Figure 4A. This PFT was mapped on all aspects, which coincides with the

Table 1. Number of Endmembers per Class Selected at Each Spatial Resolution

Class	Spatial resolution		
	20 m	40 m	60 m
Broadleaf deciduous tree	8	4	2
Needleleaf evergreen tree	14	7	6
Broadleaf deciduous shrub	6	4	4
Grass/herbaceous	10	3	2
Rock/soil	6	5	5
Total	44	23	19

observed distribution of aspen within the study area. Broadleaf deciduous shrubs are most prevalent at lower elevations on the western and northern portions of the map in Figure 4A. The grass/herbaceous PFT occurred throughout the image, but was most prevalent at higher elevations. The rock/soil class dominated at the highest elevations, but was also found where rocky outcrops intermixed with the surrounding vegetation at some lower elevations. Most of the unclassified pixels were found at high elevations where snow and exposed rock were present.

The MESMA classification results at 40 m spatial resolution (Fig. 4B) demonstrated several differences in the spatial distribution of the four PFTs and the rock/soil class. The broadleaf deciduous tree PFT was much more prevalent, reaching lower-elevation portions of the image where this PFT likely does not actually occur. Broadleaf deciduous tree appears to replace broadleaf deciduous shrub in some northern parts of the study area. This trend continues at 60 m (Fig. 4C). The spatial contiguity of the four PFTs and the rock/soil class appears reduced at 60 m, and the classes do not appear to coincide with natural topographic features as readily as they do in the 20 m classification.

Pixel-level error matrices show the details of the classification results for the three resolutions of AVIRIS images modeled by endmembers of the same resolution (Tables 2–4). Overall accuracy and kappa values were higher at 20 m resolution than at 40 and 60 m resolution (Table 5). Overall accuracy declined by almost 10% from 20 m to 40 m, and kappa declined from 0.84 to 0.72. Overall accuracy and kappa increased slightly from 40 m to 60 m. At 20 m spatial resolution, all user's accuracies (Table 6) and producer's accuracies (Table 7) exceeded 75%. User's accuracies for the needleleaf evergreen tree PFT exceeded 99% at 20 m, while producer's accuracies exceeded 90% for the two broadleaf deciduous PFTs.

Most of the user's and producer's accuracy values decreased from 20 m to 40 m. User's accuracy for needleleaf evergreen tree remained at 99%, but producer's accuracy for the same PFT declined by over 22% (Table 7). Producer's accuracies for needleleaf evergreen tree and grass/herbaceous moderately recovered from 40 m to 60 m spatial resolution, but producer's accuracies of the remaining classes declined. At 60 m spatial resolution, the number of pixels extracted from each polygon is relatively small, so a small number of misclassified pixels resulted in large changes in accuracy values. The user's accuracy for the grass/herbaceous PFT was only 53%, because

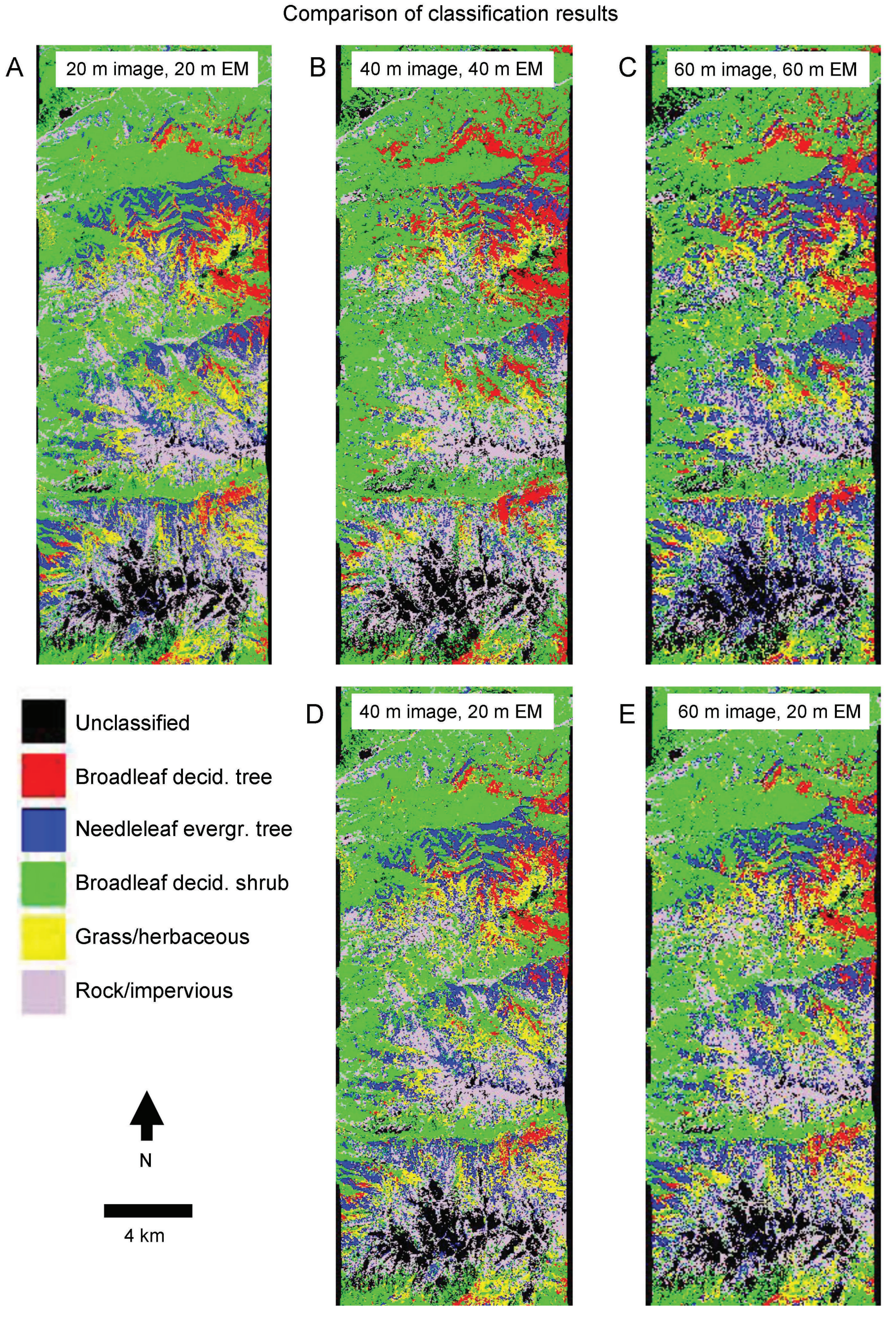

Fig. 4. Classification result of MESMA applied to the 20 m image using endmembers extracted from the same image (A), the 40 m image using endmembers extracted from the same image (B), the 60 m image using endmembers extracted from the same image (C), the 40 m image using endmembers extracted from the 20 m image (D), and the 60 m image using endmembers extracted from the 20 m image (E).

Table 2. Pixel-Level Error Matrix for the 20 m AVIRIS Image Modeled Using the 20 m Endmember Library

Classification	Reference				
	Broadleaf deciduous tree	Needleleaf evergreen tree	Broadleaf deciduous shrub	Grass/ herbaceous	Rock/soil
Broadleaf deciduous tree	403	79	21	30	0
Needleleaf evergreen tree	1	1124	3	0	6
Broadleaf deciduous shrub	7	105	1226	16	54
Ggrass/herbaceous	27	35	9	320	8
Rock/soil	0	12	2	0	752
Unclassified	5	0	2	8	113

Table 3. Pixel-Level Error Matrix for the 40 m AVIRIS Image Modeled Using the 40 m Endmember Library

Classification	Reference				
	Broadleaf deciduous tree	Needleleaf evergreen tree	Broadleaf deciduous shrub	Grass/ herbaceous	Rock/soil
Broadleaf deciduous tree	103	48	14	14	0
Needleleaf evergreen tree	0	207	0	0	2
Broadleaf deciduous shrub	0	43	294	6	14
Grass/herbaceous	8	25	2	63	3
Rock/soil	0	17	1	0	190
Unclassified	1	0	14	6	26

grass/herbaceous endmembers mapped several 60 m pixels belonging to other classes (Table 4). User's accuracy for needleleaf evergreen tree remained high (Table 6), with only 3 pixels from other classes being mapped as this PFT.

At all three spatial resolutions, broadleaf deciduous tree and grass/herbaceous endmembers mapped other classes (Tables 2–4), resulting in lower user's accuracies. Needleleaf evergreen tree and grass/herbaceous PFTs were more likely to be mapped as other classes, resulting in lower producer's accuracies. At all spatial resolutions rock/soil was the most frequently unclassified class. Rock, soil, and subdominant vegetation present in the accuracy polygons may not have been adequately represented in the training polygons due to complex local stratigraphy. Increasing the RMSE threshold would have likely reduced the number of unclassified pixels belonging to the rock/soil class.

Table 4. Pixel-Level Error Matrix for the 60 m AVIRIS Image Modeled Using the 60 m Endmember Library

Classification	Reference				
	Broadleaf deciduous tree	Needleleaf evergreen tree	Broadleaf deciduous shrub	Grass/ herbaceous	Rock/soil
Broadleaf deciduous tree	43	17	4	7	1
Needleleaf evergreen tree	1	118	1	0	1
Broadleaf deciduous shrub	1	8	120	1	3
Grass/herbaceous	4	9	14	33	2
Rock/soil	0	3	0	0	72
Unclassified	1	0	3	0	23

Table 5. Overall Pixel-Level Accuracy and Kappa for Each Modeled Image, Sorted from Highest Accuracy to Lowest Accuracy

Image resolution	Endmember resolution	Overall accuracy (%)	Kappa
20	20	87.6	0.84
40	20	86.1	0.82
60	20	83.3	0.78
60	60	78.8	0.73
40	40	77.8	0.72

Table 6. Pixel-Level User's Accuracy (in percent) for Each Combination of Image and Endmember Resolution

Image resolution	Endmember resolution	Broadleaf deciduous tree	Needleleaf evergreen tree	Broadleaf deciduous shrub	Grass/ herbaceous	Soil/rock
20	20	75.6	99.1	87.1	80.2	98.2
40	40	57.5	99.0	82.4	62.4	91.4
60	60	59.7	97.5	90.2	53.2	96.0
40	20	76.9	97.8	84.4	78.1	95.8
60	20	72.1	98.3	82.0	78.1	91.1

Applying 20 m Endmembers to Coarser Resolution Images

When the endmembers selected from the 20 m image were used to classify the 40 and 60 m images, classification results were much more similar to the 20 m classification results than when endmembers were selected at the spatial resolution of

Table 7. Pixel-Level Producer's Accuracy (in percent) for Each Combination of Image and Endmember Resolution

Image resolution	Endmember resolution	Broadleaf deciduous tree	Needleleaf evergreen tree	Broadleaf deciduous shrub	Grass/ herbaceous	Soil/rock
20	20	91.0	83.0	97.1	85.6	80.6
40	40	92.0	60.9	90.5	70.8	80.9
60	60	86.0	76.1	84.5	80.5	70.6
40	20	92.0	78.8	97.9	84.3	78.3
60	20	88.0	72.9	96.5	78.1	80.4

the 40 and 60 m images (Figs. 4D and 4E). The pixel-level error matrices show the details of the classification results when compared to the reference data (Tables 8 and 9). Low-elevation occurrence of the broadleaf deciduous tree PFT was reduced at 40 m and 60 m compared to the previous results. Areas of needleleaf evergreen tree were more continuous and consistent across spatial resolutions when the single set of endmembers selected at 20 m spatial resolution was used. Use of the 20 m endmembers on the 40 and 60 m images resulted in higher overall accuracy and kappa values (Table 5). The overall accuracy dropped by only 1.5% from 20 m to 40 m, compared to a 9.8% decrease when the 40 m endmembers were used. The overall accuracy dropped by 4.4% from 20 m to 60 m, compared to an 8.8% decrease when 60 m endmembers were used.

Decreases in user's and producer's accuracies were moderated by using the 20 m endmembers on the 40 m and 60 m spatial resolution images (Tables 6 and 7). The broadleaf deciduous tree and grass/herbaceous PFTs that exhibited the largest decreases in user's accuracy at 40 and 60 m had much smaller decreases in user's accuracy when 20 m endmembers were used (Table 6). Using 40 and 60 m endmembers resulted in user's accuracies below 60% when applied to images at those spatial resolutions, while using 20 m endmembers on the 40 m and 60 m images resulted in user's accuracies no lower than 72%. Results were less consistent for producer's accuracies (Table 7). Using 20 m endmembers on the 40 m image increased the producer's accuracies for the needleleaf evergreen tree and grass/herbaceous PFTs, but using 20 m endmembers on the 60 m image decreased producer's accuracies for the same PFTs.

Significance of Differences in Classification Accuracy

With five different classifications, a total of 10 unique comparisons between classifications can be made to determine whether kappa values for a pair of classifications are significantly different. Seven of the 10 paired comparisons had statistically significant differences in Z values (Table 10). Positive values in Table 10 indicate the classification in the leftmost column resulted in a higher kappa than the classification in the top row. Values > 1.65 or < -1.65 indicate a significant difference between the classifications with a 95% level of confidence. For the 40 and 60 m images, classifications

Table 8. Pixel-Level Error Matrix for the 40 m AVIRIS Image Modeled Using the 20 m Endmember Library

Classification	Reference				
	Broadleaf deciduous tree	Needleleaf evergreen tree	Broadleaf deciduous shrub	Grass/ herbaceous	Rock/soil
Broadleaf deciduous tree	103	19	3	9	0
Needleleaf evergreen tree	0	268	1	0	5
Broadleaf deciduous shrub	1	37	318	5	16
Grass/herbaceous	8	9	2	75	2
Rock/soil	0	7	1	0	184
Unclassified	0	0	0	0	28

Table 9. Pixel-Level Error Matrix for the 60 m AVIRIS Image Modeled Using the 20 m Endmember Library

Classification	Reference				
	Broadleaf deciduous tree	Needleleaf evergreen tree	Broadleaf deciduous shrub	Grass/ herbaceous	Rock/soil
Broadleaf deciduous tree	44	10	1	6	0
Needleleaf evergreen tree	1	113	1	0	0
Broadleaf deciduous shrub	1	21	137	3	5
Grass/herbaceous	2	4	2	32	1
Rock/soil	0	7	1	0	82
Unclassified	2	0	0	0	14

using 20 m endmembers resulted in significantly higher accuracy than using endmembers from the same spatial resolution. Moreover, there was not a significant difference between kappa values for the 40 and 60 m images when modeled by 20 m endmembers. The 20 m image had a significantly higher kappa value than the 40 m image if the 40 m image was modeled by 40 m endmembers. When the 40 m image was modeled by 20 m endmembers, the 20 m image did not have a significantly higher kappa value.

DISCUSSION

Coarsening image spatial resolution reduced classification accuracy, even when the same set of endmembers was used to model all images. Spectral mixing caused by spatial averaging increased confusion between PFTs as spatial resolution coarsened.

Table 10. Z-Statistic Results Comparing the Kappa Values from the Five Classifications[a]

	40 m modeled with 20 m endmembers	60 m modeled with 20 m endmembers	40 m modeled with 40 m endmembers	60 m modeled with 60 m endmembers
20 m modeled with 20 m endmembers	1.33	***2.49***	***7.25***	***4.59***
40 m modeled with 20 m endmembers		1.42	***4.97***	***3.36***
60 m modeled with 20 m endmembers			***2.49***	***1.68***
40 m modeled with 40 m endmembers				–0.49

[a]Significant differences are indicated in bold italic type.

Spatial averaging did not take into account the point spread function of a coarser spatial resolution sensor, and also reduced sensor noise through averaging, so classification accuracies could be lower if data from an actual 40 m or 60 m sensor were used. The characteristics of the training and accuracy polygons also affected accuracy at different spatial resolutions. Polygons were required to be at least 60 m in size and at least 75% dominated by a single PFT or land cover type. These requirements likely screened out smaller or more heterogeneous vegetation patches that could have been correctly classified at finer spatial resolution but would be incorrectly classified at coarser spatial resolution.

Coarsening the spatial resolution of the endmembers decreased classification accuracies more than coarsening the spatial resolution of the image alone. This result suggests differences in the spectral libraries created at each spatial resolution. Since image spectra were extracted from polygons with fairly homogeneous PFTs, spatial averaging of these spectra should have reduced the spectral variability within each PFT class. Class average RMSE (CAR) (Dennison and Roberts, 2003a) can be used to assess the spectral variability of endmembers within PFT classes. CAR calculates the mean RMSE of a set of endmembers by modeling all spectra from the same class or another class using a two-endmember SMA. In this case, CAR was used to find the mean RMSE of endmembers modeling all spectra within the same class. The CAR value for a class will increase as endmembers are less able to account for the spectral variability within a class (Dennison and Roberts, 2003a).

With the exception of the broadleaf deciduous shrub class, CAR increased with coarsening spatial resolution, indicating higher spectral variability at coarser spatial resolutions (Table 11). Increases in within-class spectral variability are at least partially due to spectral mixing occurring at the edges of training polygons. Pixels were extracted from polygons if their centroids were inside the polygon boundary. At coarser spatial resolutions, this makes it more likely that edge pixels will contain

Table 11. Class Average RMSE from the 20 m, 40 m, and 60 m Endmember Libraries

Endmember library	Broadleaf deciduous tree	Needleleaf evergreen tree	Broadleaf deciduous shrub	Grass/ herbaceous	Rock/soil
20 m	0.0128	0.0272	0.0466	0.0120	0.0380
40 m	0.0287	0.0226	0.0309	0.0295	0.0481
60 m	0.0103	0.0349	0.0361	0.0354	0.0549

mixed reflectance from both the targeted PFT and another PFT or land cover type. Thus, spectral mixing at the edges of polygons may have reduced classification accuracies at coarser spatial resolutions by increasing spectral variability in both the training and accuracy assessment data. One possible solution to reducing edge mixing is to buffer training polygons along their inside edges, reducing the possibility that a pixel that partially covers another PFT will get selected. However, buffering can greatly reduce the number of spectra extracted for each polygon, and eliminate smaller polygons entirely.

PFT heterogeneity and patch size will ultimately determine how well PFT mapping using imaging spectrometer data scales to coarser spatial resolutions. The large, relatively homogeneous polygons used in this study produced high accuracies even at 60 m spatial resolution. Lower accuracies are likely in ecosystems with higher spatial heterogeneity in PFTs. Given that future spaceborne imaging spectrometers are likely to map large areas of the Earth's land surface, further work should focus on assessing PFT mapping across a broad range of ecosystems and terrain characteristics. An additional challenge for a spaceborne global mapping mission is identifying appropriate PFTs that can be applied at regional-to-global scales. PFTs identified within the Wasatch Range study area may not be applicable or classifiable in other regions of North America or the world.

CONCLUSIONS

Classification of PFTs using AVIRIS data acquired over the Wasatch Range produced high overall accuracies at all spatial resolutions, but classification accuracy did decrease with coarsening spatial resolution. Spectral mixing in pixels situated on the edges of polygons likely increased the spectral variability within the 40 and 60 m endmember libraries, but declines in accuracy were moderated when endmembers were selected from the 20 m resolution image. Additional analysis using a range of polygon sizes and buffering is needed to determine whether the increased accuracy provided by higher spatial resolution endmembers is solely due to reduced edge mixing. If edge mixing is eliminated as a source of error and "more pure" higher spatial resolution endmembers are still found to confer an advantage for mapping PFTs in coarser spatial resolution images, data from finer resolution airborne or spaceborne imaging spectrometers may be valuable for creating endmember libraries for a coarser resolution global dataset. Finally, although classification accuracy is apparently reduced at coarser spatial resolutions, the tradeoffs between accuracy and global coverage may still be acceptable for providing otherwise unobtainable inputs for global-scale process modeling.

ACKNOWLEDGMENTS

We would like to acknowledge the assistance of the NASA JPL AVIRIS team, including Robert Green and Sarah Lundeen, for providing the AVIRIS data used in this study. We also thank Bob Benton, Annie Bryant, McKenzie Skiles, Jamie Turrin, and Yuan Zhang, who contributed to preliminary analysis of the AVIRIS image as part of a graduate seminar at the University of Utah. Support for this work was provided by the NASA Terrestrial Ecology program, grant #NNX08AM89G.

REFERENCES

Adams, J. B., Smith, M. O., and A. R. Gillespie, 1993, "Imaging Spectroscopy: Interpretation Based on Spectral Mixture Analysis," in *Remote Geochemical Analysis: Elemental and Mineralogical Composition*, Pieters, C. M. and P. A. J. Englert (Eds.), Cambridge, UK: Press Syndicate of University of Cambridge, 145–166.

Anderson, G. P., Felde, G. W., Hoke, M. L., Ratkowski, A. J., Cooley, T., Chetwynd, J. H., Gardner, J. A., Adler-Golden, S. M., Matthew, M. W., Berk, A., Bernstein, L. S., Acharya, P. K., Miller, D., and P. Lewis, 2002, "MODTRAN4-Based Atmospheric Correction Algorithm: FLAASH (Fast Line-of-sight Atmospheric Analysis of Spectral Hypercubes)," in *Proceedings of SPIE—The International Society for Optical Engineering*, 4725:65–71.

Asner, G. P., Jones, M. O., Martin, R. E., Knapp, D. E., and R. F. Hughes, 2008, "Remote Sensing of Native and Invasive Species in Hawaiian Forests," *Remote Sensing of Environment*, 112(5):1912–1926.

Baatz, M., Benz, U., Dehghani, S., Heynen, M., Höltje, A., Hofmann, P., Lingenfelder, I., Mimler, M., Sohlbach, M., Weber, M., and G. Willhauck, 2004, *eCognition Professional User Guide*, München, Germany: Definiens Imaging GmbHp.

Ballantine, J. A. C., Okin, G. S., Prentiss, D. E., and D. A. Roberts, 2005, "Mapping North African Landforms Using Continental Scale Unmixing of MODIS Imagery," *Remote Sensing of Environment*, 97(4):470–483.

Bobbe, T., Lachowski, H., Maus, P., Greer, J., and C. Dull, 2001, "A Primer on Mapping Vegetation Using Remote Sensing," *International Journal of Wildland Fire*, 10(3–4):277–287.

Bugmann, H., 1996, "Functional Types of Trees in Temperate and Boreal Forests: Classification and Testing," *Journal of Vegetation Science*, 7(3):359–370.

Chambers, J. Q., Fisher, J. I., Zeng, H., Chapman, E. L., Baker, D. B. and G. C. Hurtt, 2007, "Hurricane Katrina's Carbon Footprint on U.S. Gulf Coast Forests," *Science*, 318:1107.

Clark, M. L., Roberts, D. A., and D. B. Clark, 2005, "Hyperspectral Discrimination of Tropical Rain Forest Tree Species at Leaf to Crown Scales," *Remote Sensing of Environment*, 96(3–4):375–398.

Congalton, R. G., 1991, "A Review of Assessing the Accuracy of Classifications of Remotely Sensed Data," *Remote Sensing of Environment*, 37(1):35–46.

Dennison, P. E., Charoensiri, K., Roberts, D. A., Peterson, S. H. and R. O. Green, 2006, “Wildfire Temperature and Land Cover Modeling Using Hyperspectral Data,” *Remote Sensing of Environment*, 100(2):212–222.

Dennison, P. E., Halligan, K. Q., and D. A. Roberts, 2004, “A Comparison of Error Metrics and Constraints for Multiple Endmember Spectral Mixture Analysis and Spectral Angle Mapper,” *Remote Sensing of Environment*, 93(3):359–367.

Dennison, P. E., and D. S. Matheson, 2011, “Comparison of Fire Temperature and Fractional Area Modeled from SWIR, MIR, and TIR Multispectral and SWIR Hyperspectral Airborne Data,” *Remote Sensing of Environment*, 115(3):876–886.

Dennison, P. E., Nagler, P. L., Hultine, K. R., Glenn, E. P. and J. R. Ehleringer, 2009, “Remote Monitoring of Tamarisk Defoliation and Evapotranspiration Following Saltcedar Leaf Beetle Attack,” *Remote Sensing of Environment*, 113(7):1462–1472.

Dennison, P. E. and D. A. Roberts, 2003a, “Endmember Selection for Multiple Endmember Spectral Mixture Analysis Using Endmember Average RMSE,” *Remote Sensing of Environment*, 87(2–3):123–135.

Dennison, P. E. and D. A. Roberts, 2003b, “The effects of Vegetation Phenology on Endmember Selection and Species Mapping in Southern California Chaparral,” *Remote Sensing of Environment*, 87(2–3):295–309.

Diaz, S. and M. Cabido, 1997, “Plant Functional Types and Ecosystem Function in Relation to Global Change,” *Journal of Vegetation Science*, 8(4):463–474.

Diaz Barradas, M. C., Zunzunegui, M., Tirado, R., Ain-Lhout, F., and F. Garcia Novo, 1999, “Plant Functional Types and Ecosystem Function in Mediterranean Shrubland,” *Journal of Vegetation Science*, 10(5):709–716.

Everitt, J. H., Anderson, G. L., Escobar, D. E., Davis, M. R., Spencer, N. R., and R. J. Andrascik, 1995, “Use of Remote Sensing for Detecting and Mapping Leafy Spurge (*Euphorbia esula*),” *Weed Technology*, 9(3):599–609.

Hamada, Y., Stow, D. A., Coulter, L. L., Jafolla, J. C., and Hendricks, L. W., 2007, “Detecting Tamarisk species (*Tamarix* spp.) in Riparian Habitats of Southern California Using High Spatial Resolution Hyperspectral Imagery,” *Remote Sensing of Environment*, 109(2):237–248.

Johnson, J. R., Staid, M. I., Titus, T. N., and K. Becker, 2006, “Shocked Plagioclase Signatures in Thermal Emission Spectrometer Data of Mars,” *Icarus*, 180(1):60–74.

Kruse, F. A., Lefkoff, A. B., Boardman, J. W., Heidebrecht, K. B., Shapiro, A. T., Barloon, P. J., and A. F. H. Goetz, 1993, “The Spectral Image Processing System (SIPS)—Interactive Visualization and Analysis of Imaging Spectrometer Data,” *Remote Sensing of Environment*, 44(2–3):145–163.

Lavorel, S. and E. Garnier, 2002, “Predicting Changes in Community Composition and Ecosystem Functioning from Plant Traits: Revisiting the Holy Grail,” *Functional Ecology*, 16(5):545–556.

Li, L. and J. F. Mustard, 2003, “Highland Contamination in Lunar Mare Soils: Improved Mapping with Multiple End-member Spectral Mixture Analysis (MESMA),” *Journal of Geophysical Research E: Planets*, 108(6):7-1–7-14.

Li, L., Ustin, S. L., and M. Lay, 2005, “Application of Multiple Endmember Spectral Mixture Analysis (MESMA) to AVIRIS Imagery for Coastal Salt Marsh Mapping: A Case Study in China Camp, CA, USA,” *International Journal of Remote Sensing*, 26(23):5193–5207.

Martin, M. E., Newman, S. D., Aber, J. D., and R. G. Congalton, 1998, "Determining Forest Species Composition Using High Spectral Resolution Remote Sensing Data," *Remote Sensing of Environment*, 65(3):249–254.

Mundt, J. T., Glenn, N. F., Weber, K. T., Prather, T. S., Lass, L. W. and J. Pettingill, 2005, "Discrimination of Hoary Cress and Determination of Its Detection Limits via Hyperspectral Image Processing and Accuracy Assessment Techniques," *Remote Sensing of Environment*, 96(3–4):509–517.

Myneni, R. B., Dong, J., Tucker, C. J., Kaufmann, R. K., Kauppi, P. E., Liski, J., Zhou, L., Alexeyev, V., and M. K. Hughes, 2001, "A Large Carbon Sink in the Woody Biomass of Northern Forests," *Proceedings of the National Academy of Sciences of the United States of America*, 98(26):14,784–14,789.

Narumalani, S., Mishra, D. R., Burkholder, J., Merani, P. B. T., and G. Willson, 2006, "A Comparative Evaluation of ISODATA and Spectral Angle Mapping for the Detection of Saltcedar Using Airborne Hyperspectral Imagery," *Geocarto International*, 21(2):59–66.

National Research Council, 2007, *Earth Science and Applications from Space National Imperatives for the next Decade and Beyond*, Washington DC: National Academies Press.

Nemani, R. R., Running, S. W., Pielke, R. A., and T. N. Chase, 1996, "Global Vegetation Cover Changes from Coarse Resolution Satellite Data," *Journal of Geophysical Research D: Atmospheres*, 101(D3):7157–7162.

Okin, G. S., Roberts, D. A., Murray, B., and W. J. Okin, 2001, "Practical Limits on Hyperspectral Vegetation Discrimination in Arid and Semiarid Environments," *Remote Sensing of Environment*, 77(2):212–225.

Painter, T. H., Dozier, J., Roberts, D. A., Davis, R. E. and R. O. Green, 2003, "Retrieval of Subpixel Snow-Covered Area and Grain Size from Imaging Spectrometer Data," *Remote Sensing of Environment*, 85(1):64–77.

Plourde, L. C., Ollinger, S. V., Smith, M. L., and M. E. Martin, 2007, "Estimating Species Abundance in a Northern Temperate Forest Using Spectral Mixture Analysis," *Photogrammetric Engineering and Remote Sensing*, 73(7):829–840.

Powell, R. L., Roberts, D. A., Dennison, P. E., and L. L. Hess, 2007, "Sub-pixel Mapping of Urban Land Cover Using Multiple Endmember Spectral Mixture Analysis: Manaus, Brazil," *Remote Sensing of Environment*, 106(2):253–267.

Rashed, T., Weeks, J. R., Roberts, D., Rogan, J., and R. Powell, 2003, "Measuring the Physical Composition of Urban Morphology Using Multiple Endmember Spectral Mixture Models," *Photogrammetric Engineering and Remote Sensing*, 69(9):1011–1020.

Roberts, D. A., Dennison, P. E., Gardner, M. E., Hetzel, Y., Ustin, S. L., and C. T. Lee, 2003, "Evaluation of the Potential of Hyperion for Fire Danger Assessment by Comparison to the Airborne Visible/Infrared Imaging Spectrometer," *IEEE Transactions on Geoscience and Remote Sensing*, 41(6):1297–1310.

Roberts, D. A., Gardner, M., Church, R., Ustin, S., Scheer, G., and R. O. Green, 1998, "Mapping Chaparral in the Santa Monica Mountains Using Multiple Endmember Spectral Mixture Models," *Remote Sensing of Environment*, 65(3):267–279.

Thenkabail, P. S., Enclona, E. A., Ashton, M. S., and B. Van Der Meer, 2004, "Accuracy Assessments of Hyperspectral Waveband Performance for Vegetation Analysis Applications," *Remote Sensing of Environment*, 91(3–4):354–376.

Tsai, F., Lin, E. K., and H. H. Wang, 2005, "Detecting Invasive Plant Species Using Hyperspectral Satellite Imagery" in *International Geoscience and Remote Sensing Symposium (IGARSS)*, 3002–3005.

Underwood, E., Ustin, S., and D. DiPietro, 2003, "Mapping Nonnative Plants Using Hyperspectral Imagery," *Remote Sensing of Environment*, 86(2):150–161.

Ustin, S. L., DiPietro, D., Olmstead, K., Underwood, E., and G. J. Scheer, 2002, "Hyperspectral Remote Sensing for Invasive Species Detection and Mapping," in *International Geoscience and Remote Sensing Symposium (IGARSS) 2002*, 1658–1660.

Walker, B. H., 1992, "Biodiversity and Ecological Redundancy," *Conservation Biology*, 6(1):18–23.

Williams, A. P. and E. R. Hunt, Jr., 2002, "Estimation of Leafy Spurge Cover from Hyperspectral Imagery Using Mixture Tuned Matched Filtering," *Remote Sensing of Environment*, 82(2–3):446–456.

Woodward, F. I. and W. Cramer, 1996, "Plant Functional Types and Climatic Changes: Introduction," *Journal of Vegetation Science*, 7(3):306–308.

Youngentob, K. N., Roberts, D. A., Held, A. A., Dennison, P. E., Jia, X., and D. B. Lindenmayer, 2011, "Mapping Two Eucalyptus Subgenera Using Multiple Endmember Spectral Mixture Analysis and Continuum-Removed Imaging Spectrometry Data," *Remote Sensing of Environment*, 115(5):1115–1128.